Natural convection heat transfer from a ribbed vertical plate: Effect of rib size, pitch, and truncation

Giovanni Tanda, Essam Nabil Ahmed, Alessandro Bottaro

Highlights:

- Free convection heat transfer from a ribbed vertical plate was experimentally studied.
- The effect of rib size, pitch and truncation is investigated.
- Continuous ribs negatively affect heat transfer performance, compared to a smooth plate.
- Staggered truncated ribs significantly enhance heat transfer from the baseplate.
- An optimal length of rib segments for truncated ribs was found.

Manuscript File Click here to view linked References

Natural convection heat transfer from a ribbed vertical plate: Effect of rib size, pitch, and truncation

Giovanni Tanda[1*], Essam Nabil Ahmed[2], Alessandro Bottaro[2]

[1]DIME, Università degli Studi di Genova, via Montallegro 1, 16145, Genova, Italy
[2]DICCA, Università degli Studi di Genova, via Montallegro 1, 16145 Genova, Italy
*Corresponding Author, e-mail: giovanni.tanda@unige.it

Abstract

Buoyancy-induced flows over ribbed vertical surfaces involve complex thermal and dynamic interactions between the mainstream and the surface texture, yielding contrasting effects on the heat transfer performance of the heated plate; proper analysis of the overall effect on the heat transfer rate is essential for efficient operation and optimization purposes. The present work pursues an insight into the different factors controlling this problem. Natural convection heat transfer from a vertical plate of 0.5 m height, regularly roughened with wooden transverse square ribs, is experimentally investigated. The surface temperature of the baseplate is varied so that a range of the plate Rayleigh number (Ra) from 3.4×10^8 to 4.9×10^8 is covered. The density of the roughness pattern and the rib pitch-to-height ratio (*P/e*) are varied by changing the number of ribs attached to the surface (from 10 to 40 rib rows) and using three different square cross-sections (of side lengths 2, 3, or 5 mm). The experimental work relies on the schlieren optical technique, through which the thermal boundary layer is visualized and the Nusselt number distribution is acquired. Analysis of the results reveals that enhancement of the local Nusselt number, relative to a corresponding smooth surface, may be attained only at the central part of the inter-rib region; this occurs exclusively for relatively large values of *P/e*. At a later stage, the effectiveness of rib truncation in enhancing the heat transfer from the baseplate is explored. Three staggered arrangements are considered, by varying the number of rib segments per row, and heat transfer enhancement, sensitive to the number of rib segments per row, is found. This paper also provides insight into the role of thermal-field disturbances close to turbulent transition, and sheds light on the potential of truncated ribs to amplify such perturbations.

Keywords: Heat transfer, Natural convection, ribbed surface, schlieren, vertical plate, field disturbances

Nomenclature

e	rib size [m]
g	gravitational acceleration [m s^{-2}]
h	heat transfer coefficient [W m^{-2} K^{-1}]
H	plate height [m]
k_{air}	air thermal conductivity [W m^{-1} K^{-1}]
$k_{air,w}$	air thermal conductivity at the wall temperature [W m^{-1} K^{-1}]
k_{rib}	thermal conductivity of ribs [W m^{-1} K^{-1}]
K	constant in Eq.(2) [m K]
l	length of rib segments [m]
L	plate spanwise length [m]
N	number of rib rows
Nu	Nusselt number based on plate height, Eq.(4)
Nu_x	Nusselt number based on vertical coordinate x, Eq.(6)
P	rib pitch [m]
Ra	Rayleigh number based on plate height, Eq.(3)
Ra_x	Rayleigh number based on vertical coordinate x, Eq.(5)
T_{air}	ambient air temperature [K]
$T_{rib,w}$	rib surface temperature [K]
T_w	plate surface temperature [K]
x, y, z	vertical, normal, and spanwise coordinates [m]

Greek symbols

α	air thermal diffusivity [m^2 s^{-1}]
α_y	light ray angular deflection [rad]
$\alpha_{y,w}$	angular deflection of a light ray passing in the vicinity of the wall [rad]
β	coefficient of thermal expansion [K^{-1}]
ε	thermal emittance of aluminium surface

ε_{rib} thermal emittance of rib surface

v air kinematic viscosity [$m^2\ s^{-1}$]

1. Introduction

Natural convection heat transfer is a simple and reliable mechanism that does not require active devices such as fans or pumps to promote fluid motion. The effectiveness of natural convection is limited by the lower heat transfer coefficients (relative to forced convection) associated with the low buoyancy-induced flow rates. Strategies to enhance the heat transfer rate from a vertical surface include the addition of fins (which basically increase the heat transfer surface area) or large-scale roughness elements such as surface protrusions (with the purpose of increasing the heat transfer coefficient). In some applications (electronic equipment, building facades) protrusions exist naturally. Roughness elements affect the heat transfer effectiveness due to the surface alteration and the possible premature transition to turbulence. Fuji et al. [1] were among the first to investigate the influence of various surface roughness elements on natural convection. Their experiments, conducted for water and oil flowing along a vertical cylinder, revealed little variations in heat transfer coefficient compared with the smooth surface (with slight reductions for water and slight increases for oil) and no effect of roughness on the upper limit of the laminar region. Bhavnani and Bergles [2] studied the effect of repeated square ribs (of low and high thermal conductivity) and steps on natural convection heat transfer from a vertical isothermal surface. They found a substantial reduction of heat transfer performance associated with ribs due to the stagnation zone induced downstream and upstream of each rib (especially when the ribs have high thermal conductivity) and an increase in the heat transfer rate of up to 23% (as compared with a plain surface of equal projected area) for properly sized stepped surfaces. A few years later, Tanda [3] found that repeated, high-thermal-conductivity, square ribs reduce heat transfer performance in asymmetrically heated vertical channels (both in terms of average heat transfer coefficient and heat transfer rate), particularly when the channel is narrow. The use of low-thermal-conductivity ribs yielded local heat transfer coefficients higher than that for a smooth surface, at the same elevation, just downstream of the ribs (where the main flow reattachment to the wall occurs), while, on average, the heat transfer performance even with low-thermal-conductivity ribs was degraded [4]. Studies documented in Refs. [2−4] were conducted experimentally, using air as the working fluid at a relatively low Rayleigh number (of the order of 10^7), well within the laminar regime. More recently, Hærvig and Sørensen [5] numerically studied the effect of zigzag-shaped ribs, finding, again for air in the laminar regime, an increase in average heat transfer coefficient by more than 4% (compared to the flat surface) and more than 11% when accounting for the increase in heat transfer area. Nghana et al. [6] performed numerical simulations of turbulent natural convection in vertical and inclined channels with repeated square, triangular, and semi-circular ribs; they found significant heat transfer enhancements compared with the smooth channel, with the triangle-shaped ribs giving the best heat transfer performance. Based on the available studies of natural convection heat transfer in vertical channels or along unbounded vertical surfaces, the presence of repeated protrusions negatively affects the heat transfer performance (square ribs) or leads to little enhancements (steps and zigzag-shaped ribs) within the laminar regime, while they are more effective in the turbulent regime.

Even though some literature studies (e.g., refs. [7, 8]) suggest that large-scale roughness elements can trigger an early transition to turbulence, to the authors' best knowledge no systematic studies on natural convection heat transfer from vertical surfaces with repeated ribs addressed this issue, and few experimental and numerical results (for a limited number of geometries) are available either in the laminar or in the fully turbulent flow regime. This means that there is no evidence, in the literature, of premature transition to turbulence induced by repeated ribs or by macro-roughness elements of different shape and size.

A common practice to promote turbulence and heat transfer enhancement in forced convection is to use broken ribs, periodically deployed on the heat transfer surface. Broken ribs perform better than continuous ribs due to the higher turbulence levels induced (see, for instance, Cavallero and Tanda [9]). However, the fluid motion under free convection conditions is not externally imposed but derives from a balance between buoyancy and viscous forces; therefore, turbulence promoters, which have proved to be effective in forced convection, may induce a weak buoyant flow in free convection and fail to yield premature transition to turbulence. Onbasioglu and Onbaşıoğlu, [10] considered the effect of two truncated ribs of lengths equal to 67% of the surface width and placed staggered on the baseplate. Experiments were performed by varying the height and the inclination angle of the ribs. Imbriale et al. [11] experimentally investigated the effect of single or two staggered rows of ribs inclined at different angles and single or two staggered rows of V-shaped ribs. Both studies [10, 11] indicated that ribs provide significant improvements in local and average heat transfer coefficient (compared with the flat vertical surface), even though the flow regime was laminar. Being able to favourably redirect the flow, interrupted roughness elements yield a favourable flow pattern, reducing the impact of inactive heat transfer regions typically occurring immediately upstream and downstream of continuous rib. Smirnov et al. [12] numerically found that a couple of short and aligned ribs were able to trigger transitional processes in the free convection boundary layer.

Based on the above discussion of the literature, some issues remain unresolved. For instance, the survey of the literature did not reveal any systematic analysis concerning the effects of the main geometric parameters of ribs on heat transfer from a vertical plate. At the same time, the potential of triggering an early transition of the boundary layer has been previously unaccounted for, and the practice of interrupting the ribs to pursue the enhancement of the heat transfer performance has not been unveiled until now. To address these issues, in this work experiments have been performed to investigate natural convection heat transfer from an isothermal vertical plate with continuous square ribs having different size (from 2 to 5 mm) and pitch (from 12.5 to 50 mm), varying the wall-to-ambient temperature difference to achieve thermal conditions not far, for the smooth plate, from the upper threshold of the laminar flow regime. For the intermediate values of the rib size (3 mm) and rib pitch (25 mm), continuous ribs have been replaced by truncated ribs, having 3, 6, or 12 segments per row and attached in a staggered arrangement. A schlieren optical apparatus was employed to gain qualitative and quantitative information on heat transfer characteristics; the optical field encompassed the top 15 cm of the heated plate (out of the 50 cm overall height), where the onset of transition to turbulence, if any, is likely to be observed.

2. Experimental setup and procedure

The test surface was an aluminium plate, 0.5 m high, 0.3 m large, and 0.005 m thick, connected to a plane electrical heater. Since the high thermal conductivity of aluminium and the relatively large plate thickness promote an efficient redistribution of heat by conduction within the plate, the plate material was expected to be virtually isothermal. The heater-plate assembly, suspended at about 1.5 m from the floor, was insulated on one side in order to convey as much heat flux as possible towards the side exposed to the ambient air. To avoid significant sidewise air entrainment and minimize disturbances from the environment, the heated plate was bounded on both sides by two glasses (10 cm long and 50 cm high), and shrouded by a frontal polystyrene wall, placed at a distance from the heated plate approximately equal to half of the plate height. In such a way, the buoyant airflow, at ambient temperature, is mainly allowed to enter the test section from the bottom side and exit from the upper side after having flowed along the heated surface. The plate temperature was evaluated as the average among the readings given by several 0.5 mm-dia thermocouples (calibrated to ± 0.1 K) embedded at different plate elevations through small holes drilled into the material. The ambient air temperature was calculated by averaging the readings of three thermocouples situated below the heated plate.

Repeated ribs, of square cross-section, were attached to the heated plate in order to evaluate their effect on heat transfer performance. Prior experiments performed by Tanda [3, 13] for rib-roughened vertical plates, with air or water as convective fluid, considered metallic ribs integral to the baseplate to guarantee the absence of thermal contact resistance. However, the fabrication of such test sections is very expensive and does not permit a systematic study of the effect of the main geometric parameters. For this reason, ribs were made of wood, due to the low cost and the ease of cutting and application. Three different rib sizes were considered, specifically e = 2, 3, and 5 mm, where e is the side length of the ribs. Regardless of the rib size, a different number of rib rows (N = 10, 20, or 40) were regularly deployed along the plate surface height. The majority of experiments were conducted with continuous ribs. Additional tests were subsequently performed with truncated ribs; i.e., rows of three, six, or twelve segments periodically arranged in a staggered arrangement. Details of rib configurations are reported in Table 1 and Fig.1.

Table 1. Description of rib configurations and main geometric parameters.

Rib type	Number of rib rows N	e (mm)	P(mm)	l(mm)	Number of truncated ribs per row	P/e	e/H	l/L
continuous	10	2	50	-	-	25	4×10^{-3}	-
continuous	20	2	25	-	-	12.5	4×10^{-3}	-
continuous	40	2	12.5	-	-	6.25	4×10^{-3}	-
continuous	10	3	50	-	-	16.67	6×10^{-3}	-
continuous	20	3	25	-	-	8.33	6×10^{-3}	-
continuous	40	3	12.5	-	-	4.17	6×10^{-3}	-
continuous	10	5	50	-	-	10	0.01	-
continuous	20	5	25	-	-	5	0.01	-
continuous	40	5	12.5	-	-	2.5	0.01	-
truncated	20	3	25	50	3	8.33	6×10^{-3}	0.1667
truncated	20	3	25	25	6	8.33	6×10^{-3}	0.0833
truncated	20	3	25	12.5	12	8.33	6×10^{-3}	0.0417

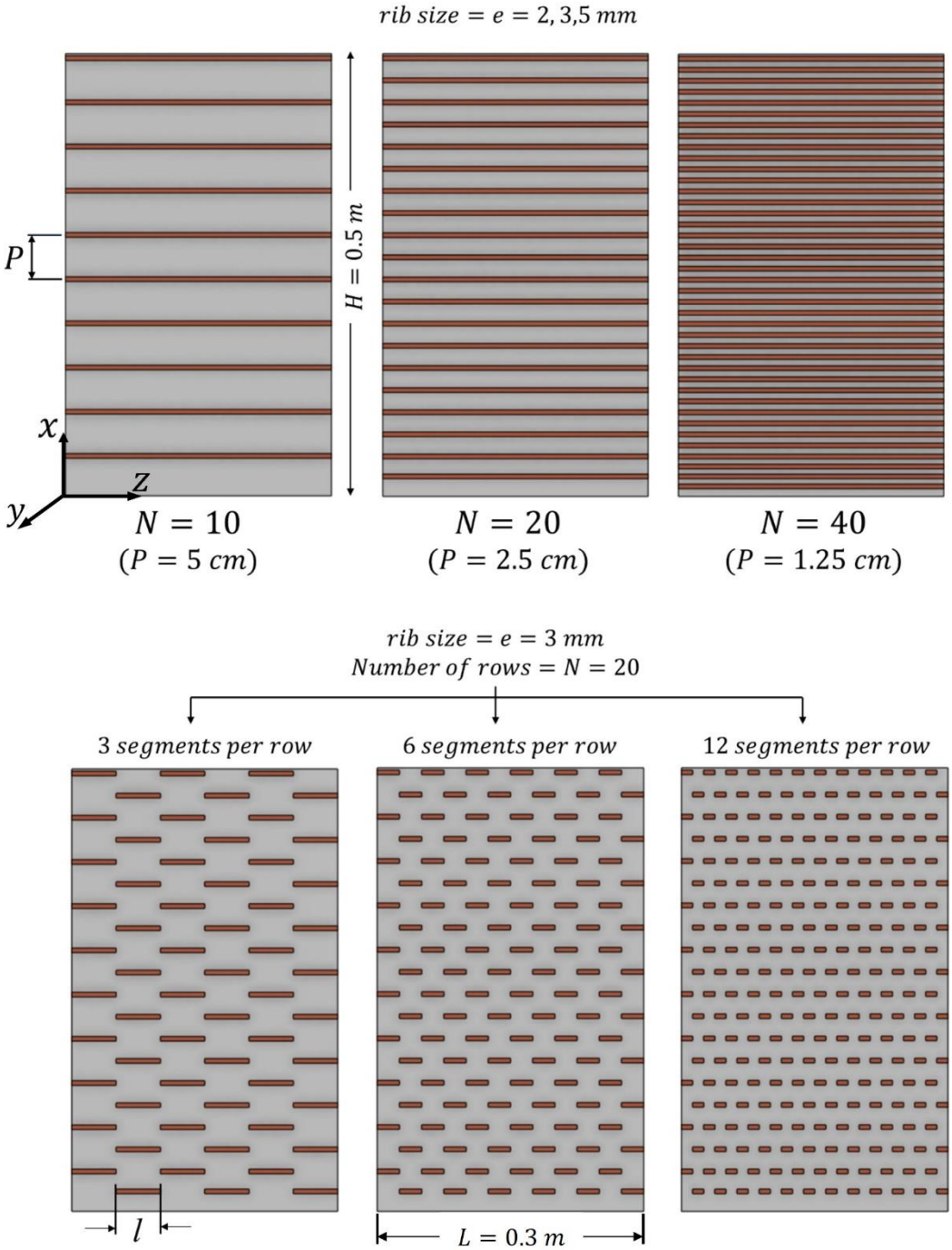

Figure 1. Sketch of the heated plate (frontal view): continuous ribs at different pitch *P*, with *N* representing the number of rib rows (top), truncated ribs of different length *l* and different number of segments per row (bottom). *H* is the vertical plate height, *L* is the spanwise length of the plate, and *e* is the size of the square ribs.

A schlieren optical system was used to visualize the thermal boundary layer and to evaluate the local, natural convection heat transfer coefficient. Optical methods are extremely versatile tools for making quantitative measurements of thermal phenomena because they allow a real-time, non-intrusive analysis over the whole optical field [14, 15]. A large variety of optical techniques are

currently employed in experimental heat transfer and fluid flow, such as the index-of-refraction optical methods. In this category of methods, among which interferometry and schlieren, the index of refraction (or its spatial derivative) of a medium is measured, and from this the temperature distribution through the medium is determined. Some applicative examples of these techniques, even in parallel, for gases and liquids, are provided in [16−23]. An exhaustive description of the schlieren apparatus employed is given in refs. [3, 4, 13, 24−27]. Basically, it consists of a white light beam (composed of parallel rays) crossing the test section, a concave mirror (i.e., the schlieren mirror), which focuses the light onto its focal plane (i.e., the cut-off plane), a filter, and a camera to acquire a real image of the test section. As shown in Fig.2, when a focal filament (for instance, a thin dark strip or wire) is used as a filter, and no thermal gradients are present in the air crossed by the light beam, all light rays are intercepted by the filter when it is placed on the focus of mirror (and the image formed on the camera will be uniformly dark). In this work, the filter has been obtained by photographing a violet strip using a slide film. The slide produced in this manner, consisting of a 370 μm-wide, transparent, violet band, was directly used as focal filament filter. When thermal gradients (in the *y*-direction of Fig.2) are present, individual light rays undergo angular deflections whose extent is related to the magnitude of the gradient; consequently, the corresponding spots appear bright in the camera, permitting a reliable visualization of the thermal boundary layer (more precisely of all air particles with a non-zero thermal gradient). The angular deflection α_y of a given light ray (i.e., passing through a given point of coordinates *x*, *y*) can be measured by moving the filter (connected to a micrometer) along the focal plane of the schlieren mirror until the point of interest appears coloured by the same colour adopted for the filter (violet). It can be demonstrated [28] that the angular deflection α_y is given by the ratio between the filter displacement and the focal length of the mirror (since the angular deviation is small, $\tan \alpha_y \approx \alpha_y$).

The local heat transfer coefficient is introduced, conventionally, as follows

$$h = -k_{air,w} \frac{(\partial T/\partial y)_w}{T_w - T_{air}} \tag{1}$$

where T_w and T_{air} are the plate wall and the ambient air temperatures, respectively, $(\partial T/\partial y)_w$ is the air temperature gradient, in the direction *y* normal to the heated plate, evaluated at the wall, and $k_{air,w}$ is the air thermal conductivity evaluated at the wall temperature. Due to the relation between angular deflection of light and thermal gradient of the crossed fluid, the heat transfer coefficient *h* can be directly calculated by measuring the deflection of light passing in the vicinity of the wall at the desired location, using the following formula (see, for instance, ref.[3])

$$h = k_{air,w}\, \alpha_{y,w}\, T^2_w \,/\, [\, K\, (T_w - T_{air})] \tag{2}$$

where $\alpha_{y,w}$ is the angular deflection, along the *y*-direction, of the light ray passing in the vicinity of the wall (i.e., at $y = 0$), and *K* is a constant (equal to about 0.024 m K in these experiments), which depends on some air properties (Gladstone-Dale and ideal gas constants, index of refraction, pressure) and the length of the plate in the direction of light beam propagation (*z*-coordinate of Fig.2). Eq.(2) provides the heat transfer coefficient for a vertical surface, which depends of the thermal gradients in the *y*-direction. In principle, since the focal filament is mounted on a holder able to rotate through an arbitrary angle on the focal plane of the schlieren mirror, the technique allows light deflections along any direction (on a plane normal to the light beam propagation) to be detected. In this research, attention is focused on vertical inter-rib regions (and not, for instance, on horizontal sides of ribs);

hence, the angular deviation along the *y*-direction is the only optical data on which the heat transfer coefficient depends.

Moreover, even though the schlieren technique may exploit, in some circumstances, a tomographic treatment of optical data to get local temperature or heat transfer coefficient results for three-dimensional flows [29], Eq.(2) assumes the thermal field to be two-dimensional, i.e., independent of the *z*-coordinate; otherwise, it is still valid but the calculated heat transfer coefficient corresponds to the value averaged along the plate spanwise length *L*, that is the plate dimension along the *z*-coordinate. This means that any three-dimensional feature of the flow emerging from the insertion of ribs can be observed only on a line-averaged basis. To partially overcome this issue, schlieren measurements were supplemented by the detection of air temperature fluctuations in the boundary layer by using a miniature thermocouple with an exposed junction, able to travel along the direction normal to the plate surface and to be located at any arbitrary position along the vertical and spanwise coordinates. A National Instrument acquisition unit (NI PXIe-1078 equipped with a NI TB-4353 module) was used to acquire the air temperature measurements at a frequency of 50 Hz.

The uncertainty in the results (at the 95% confidence level) was evaluated based on the root-sum-square of the contributions made by the uncertainties in each of the individual measurements. The details of the procedure followed for the evaluation of the experimental uncertainty are provided in previous literature studies, for instance refs. [3, 24, 25]. The main source of error in the calculation of the local heat transfer coefficient *h*, according to Eq.(2), is associated with the light ray displacement readings (i.e., the filament displacement in Fig.2). As reported by Tanda [3], the accuracy of the measurement of the light ray displacement improves as its value increases. For the present experiments, the light displacement at the focal plane of the schlieren mirror was typically between 3.5 and 1.5 mm, with associated errors ranging from 9 to 14%, increasing with the reduction of the light ray displacement. As errors in the wall-to-fluid temperature difference are accounted for, the uncertainty in *h* (and in Nusselt number) values falls into the ±10−15% range, while the uncertainty in Rayleigh number is estimated to be ±5%.

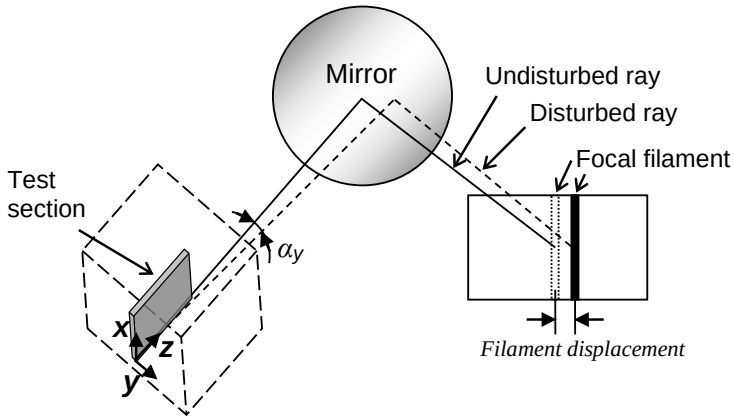

Figure 2. Quantitative schlieren (focal filament method): the angular deflection of perturbed light rays is detected by shifting the focal filament filter in the focal plane of the schlieren concave mirror.

Tests were carried out by delivering electrical power to the heater through a DC power supply, adjusting the input voltage in order to achieve the desired wall-to-fluid temperature difference. The degree of temperature uniformity of the plate was typically within ± 3% of the mean wall-to-ambient temperature difference. The plate surface exchanges heat with the environment by natural convection and radiation. For the surface regions not covered by ribs, the radiant component is expected to be low, due to the low thermal emittance of aluminium ($\varepsilon \approx 0.1$). Moreover, the schlieren method detects the air thermal gradient in the vicinity of the wall, which is unaffected by radiation; it is worth noting that radiation measurement or calculation does not contribute to the evaluation of the convective heat transfer coefficient from Eq.(2), keeping in mind that the input power is adjusted to establish the required wall-to-ambient temperature difference, for all the cases considered, regardless of variations in the heat dissipated by radiation. The ribs glued to the aluminium plate have a low thermal conductivity ($k_{rib} \approx 0.1$ W/m K) but a high emittance ($\varepsilon_{rib} \approx 0.9$); hence, the amount of heat dissipated, by convection and radiation, from the ribs' surfaces is not negligible. In fact, measurements of surface temperature $T_{rib,w}$ of rib tips, by an infrared camera, revealed values not far from the aluminium surface temperature T_w; in dimensionless terms, $(T_{rib,w} - T_{air})/(T_w - T_{air})$ ranged from 0.8 for the smaller ribs (e = 2 and 3 mm) to 0.7 for the larger ribs (e = 5 mm). Increasing the rib length leads to a reduction of the fin efficiency evaluated according to the one-dimensional fin model (and considering the rib as a small fin) and thus to a larger base-to-tip temperature drop. Schlieren measurements targeted only the baseplate regions not covered by ribs, ignoring any heat transfer contribution arising from the ribs' surfaces.

After the initiation of each test, steady state was achieved in about 6−7 hours. At the end of the test, air and wall temperatures were acquired and schlieren measurements were performed. Since the optical field encompassed a circular region having a diameter of about 20 cm, measurements of the angular deflection of light rays and visualization of the thermal boundary layer were limited to the top third of the heated plate, where transition to turbulence, if any, is more likely to occur. Measurements of air temperature inside the boundary layer were performed for a number of representative tests, over a time period of about 15 minutes, at different distances from the plate surface and locations along the vertical and spanwise directions.

The Rayleigh and Nusselt numbers, based on the plate height H or the local vertical position x, are determined from

$$Ra = \beta\, g\, (T_w - T_{air})\, H^3 / (\nu\, \alpha) \tag{3}$$

$$Nu = h\, H / k_{air} \tag{4}$$

$$Ra_x = \beta\, g\, (T_w - T_{air})\, x^3 / (\nu\, \alpha) \tag{5}$$

$$Nu_x = h\, x / k_{air} \tag{6}$$

where h is the local heat transfer coefficient, given by Eq.(2), g is the gravitational acceleration, and β, α, ν, and k_{air} denote the coefficient of thermal expansion, the thermal diffusivity, the kinematic viscosity, and the thermal conductivity of air, respectively. Air properties have been evaluated at the film temperature given by $(T_w + T_{air}) / 2$, except for β, evaluated at the ambient air temperature, as suggested in [30, 31].

For each rib configuration, the wall-to-fluid temperature was varied from 32 to 51 K in order to span the range of *Ra* from 3.4 to 4.9 × 10^8. Each test, at a given wall-to-fluid temperature difference, was repeated from 2 to 5 times and local heat transfer results were averaged among identical tests to reduce the random error.

3. Results and discussion

In this section, experimental results are presented, for the smooth plate and for each rib configuration considered. First, attention is focused on the effect of the rib size and the rib pitch on local heat transfer results. Second, the effect of rib truncation is investigated. Third, the intensity of air temperature fluctuations in the boundary layer is presented and discussed, together with qualitative visualizations of the flow in the boundary layer.

3.1 Nusselt number results

3.1.1 The smooth plate

Heat transfer results for the smooth heated plate, in terms of the Rayleigh and the Nusselt numbers based on local elevation *x*, are summarized in Fig.3. The same plot reports the analytical solution by Ostrach [32] for a vertical isothermal flat plate and air as the convective fluid, as well as other experimental data extracted from Bhavnani and Bergles [2] (by holographic interferometry) and Tanda [3] (by schlieren technique, same apparatus as in the present contribution).

Ostrach's theoretical solution pertains to the laminar regime and therefore its application requires no evidence of transitional events. Interpretation of transition was provided by Godaux and Gebhart [33] who found a distinct thermal transition mechanism. The first signs of turbulent disturbances appear in the velocity boundary layer without alteration of the temperature profile from the laminar form until reaching a point, further downstream, where the velocity disturbances become strong enough to change the temperature profile (the onset of thermal transition). The thermal transition region ends with the development of a completely turbulent boundary region where all flow variables fluctuate randomly. Nevertheless, no clear definition of the parameters ruling the transition of the buoyancy-driven flow over a vertical isothermal plate is apparent from the literature. Bejan and Lage [34] showed that the Grashof number (and not the Rayleigh number = Grashof number × Prandtl number) marks the transition in all fluids, with a value of order 10^9 at the beginning of transition (i.e., Rayleigh number of 0.7 ×10^9 when air is the convective fluid). Cheesewright [35], underlining the arbitrary nature of former attempts to specify beginning and end of transition, indicated a Grashof number of 2 ×10^9 as the condition at which significant fluctuations first appear in the boundary layer without significant changes in the mean temperature profiles or in the trend of heat transfer data; major changes in mean temperature profiles and heat transfer rates were found to appear at a Grashof number of 5 × 10^9 and up to 8 ×10^9; the amplitude of temperature fluctuations then decreased with the Grashof number from 8 ×10^9 to 2 ×10^{10}, while beyond the last threshold it remained approximately constant (meaning that the fully turbulent regime had been reached). It is worth noting that the large disagreements in the experimental evaluation of the critical Grashof number found in the literature suggest that results may depend on local conditions and the method of observation or that other quantities, instead of the Grashof number, can be more suitable to identify changes in flow regime,

like, for instance, the total amount of thermal energy given to the boundary layer by the heated surface up to the current elevation, as suggested in [33].

Inspection of Fig. 3 shows that the present experiments fall in the last decade (10^8 to 10^9) of the abscissa (Ra_x), not far from the onset of transitional regime for air (according to the general consensus emerging from the literature). A deviation of measured data, from Ostrach's solution, in the +20 to +30% range was found, even though experiments were performed in a large, isolated room, without windows and openings to the external environment, with good thermal stability and hosting only the experimental facility used for these experiments. This circumstance was observed also by other experimentalists (e.g., [2], [35]), especially towards large values of Ra_x, when the transition to turbulence was approached. According to Bhavnani and Bergles [2], experimental uncertainty and external disturbances are possible causes of these discrepancies, while Cheesewright [35] stated that uncontrolled thermal gradients in the laboratory room may trigger large-scale air currents, yielding increased heat transfer at large Rayleigh numbers. Ostrach [32] attributed the unsatisfactory agreement between his laminar theory and experimental data from the literature to disturbances induced by the slight turbulence in the room air. Schaub et al. [36] found that the Nusselt number (averaged from the leading edge to the current elevation) can be experimentally overestimated up to 29% (compared with Churchill and Chu correlation [37]) just at the upper limit of the laminar regime, in line with the deviation resulting from the present experiments.

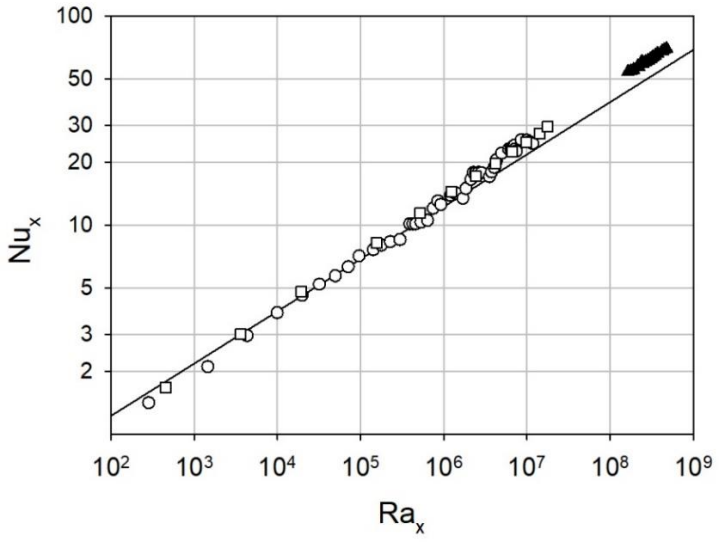

Figure 3. Local Nusselt number versus local Rayleigh number for a smooth, isothermal, vertical plate: comparison between Ostrach's solution ([32], solid line), literature results (empty circles [2], empty squares [3]) and present results (filled triangles).

3.1.2 Effect of rib size

Figure 4 illustrates the local Nusselt number distributions along the inter-rib regions of the heated plate, for a normalized elevation x/H from 0.7 to 1.0. Each plot compares the Nusselt number (Nu) for three values of the rib size e at a given Rayleigh number and rib pitch (i.e., number of rib rows N). The corresponding results over the smooth surface are also plotted. Regardless of the rib size, the

measurement points inside each inter-rib region (five for N = 10, four for N = 20, and three for N = 40) were taken at fixed locations, as it appears from inspection of the figure.

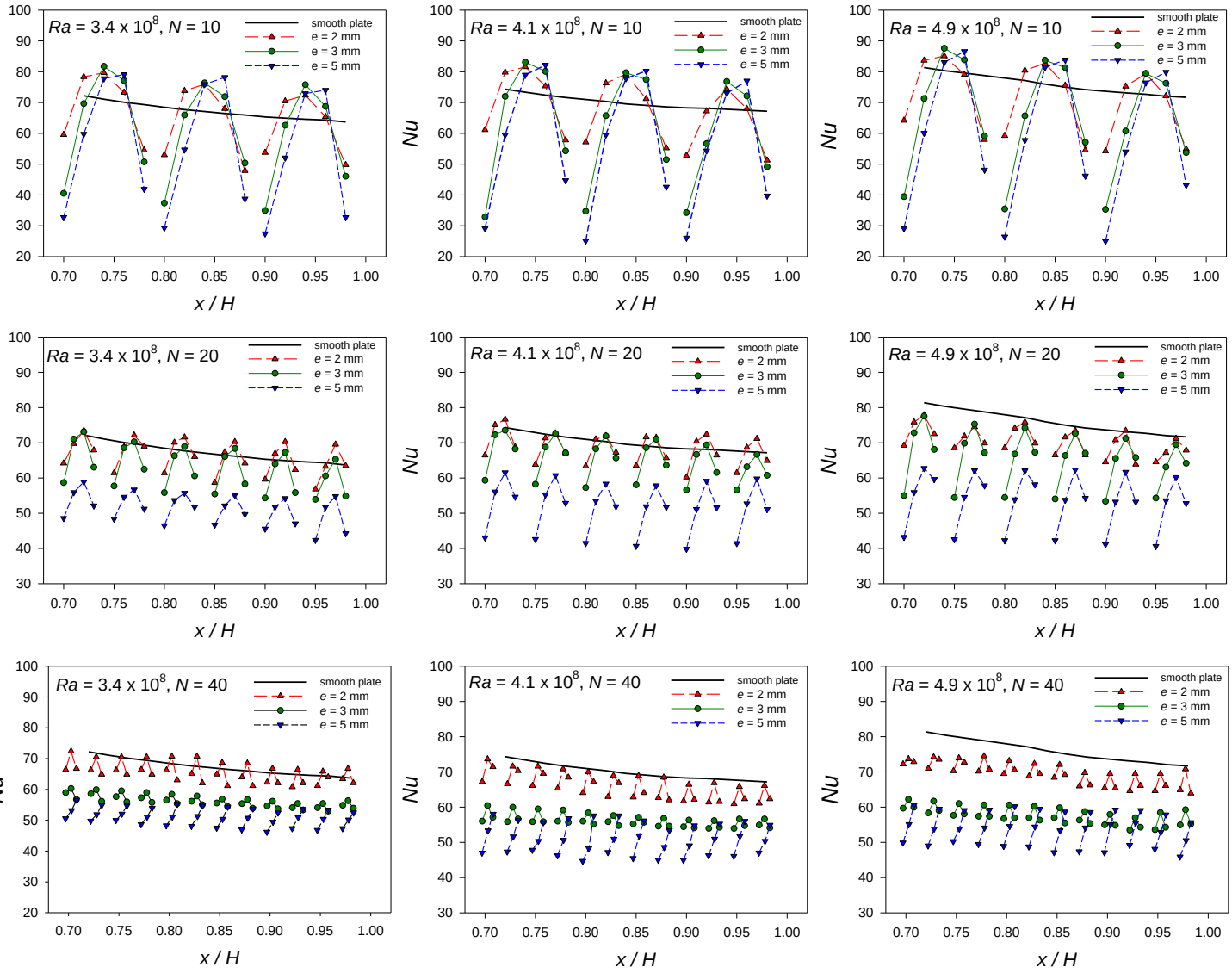

Figure 4. Nusselt number for ribbed (continuous ribs) and smooth plate: effect of the rib size.

When ribs are sparse (N = 10), heat transfer enhancement, relative to the smooth plate, is noticed in the central part of each inter-rib region, while marked reductions occur immediately downstream and upstream of each rib. As described in the literature [2−4, 38], stagnation zones up- and downstream of the ribs are responsible for local heat transfer degradation while local enhancement is found where the main flow washes the inter-rib region. The primary effect of the increased size of the ribs is the extension of the stagnation zone downstream of each rib; as a consequence, as the rib size e is increased from 2 to 5 mm, local Nu values downstream of each rib are markedly decreased and the relative maximum in the inter-rib region (whose value is poorly affected by the rib size) moves towards the downstream rib. Ribs of the lowest size (e = 2 mm) still perform better than others when they are more densely packed on the heated plate (N = 20 and 40); here the effect of the rib size is more evident, with heat transfer performance progressively degrading as the rib size is increased.

3.1.2 Effect of rib pitch

Nusselt number data have been rearranged in Fig.5 to highlight the effect of the rib pitch (i.e., the number of rib rows N). Inspection of the figure reveals that densely packing the ribs has a negative impact on the heat transfer performance, especially for the highest rib size (e = 5 mm). It is worth noting that, for e = 5 mm and N = 40, within the limits of the low number of measurement points in each inter-rib region, the ascending-descending trend of local Nu values is not observed but Nu monotonically increases along each inter-rib region; it is conjectured that, due to the reduced space between ribs (only 7.5 mm), a single weak recirculating cell is trapped inside the inter-rib region.

With Table 1 in mind, the combination of rib size and rib number which leads to a local heat transfer enhancement, limited to the central part of the inter-rib region, corresponds roughly to a rib pitch-to-height ratio P/e larger than 10. A relatively low value of P/e (say $\leq$ 5), a parameter that captures the effect of rib size and pitch, negatively affects the heat transfer performance along the entire inter-rib surface.

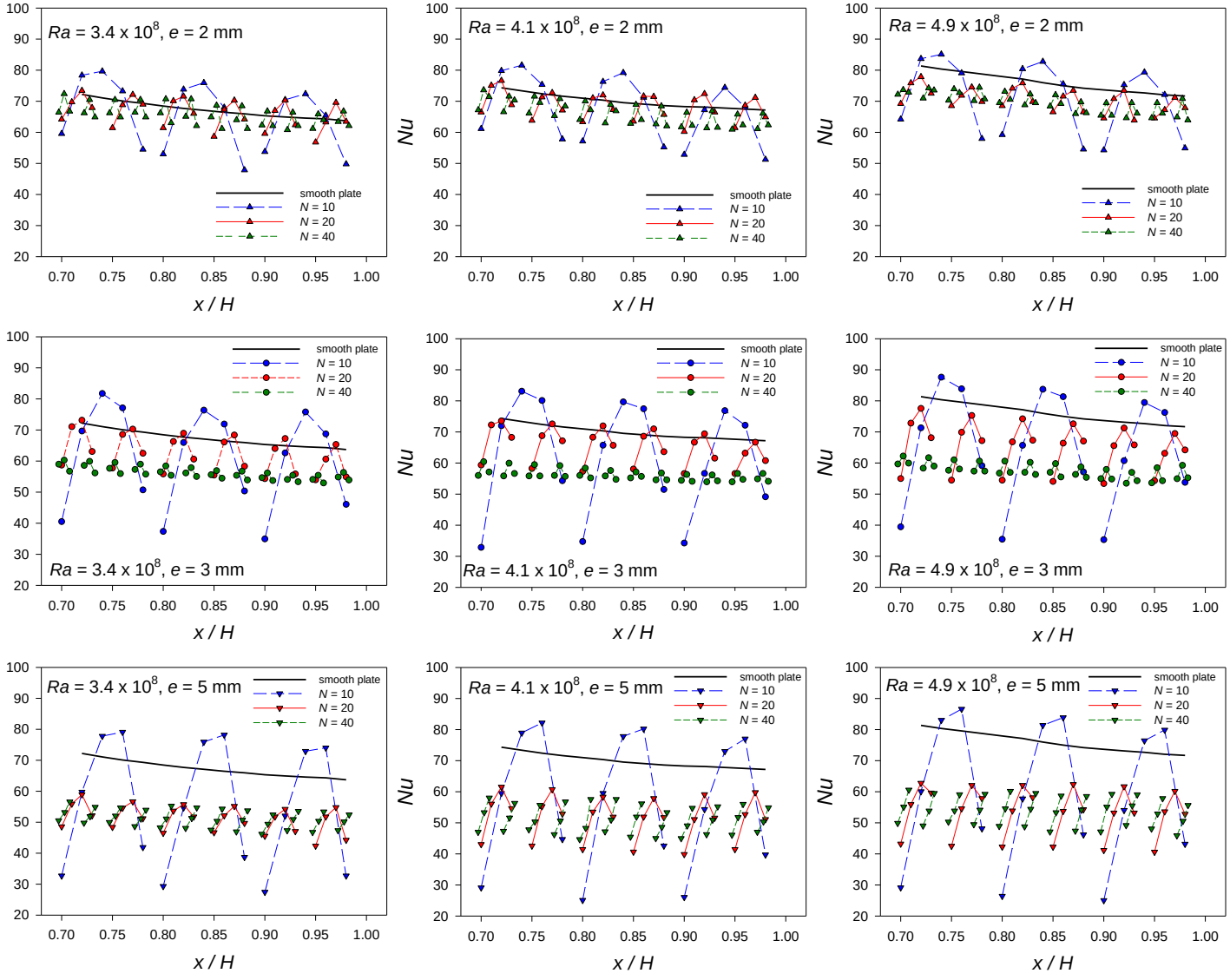

Figure 5. Nusselt number for ribbed (continuous ribs) and smooth plate: effect of the rib pitch (i.e., the number of rib rows).

3.1.3 Effect of rib truncation

Since the heat transfer enhancement, relative to the smooth plate, is the primary objective of this study, continuous ribs have been replaced by truncated ribs, seeking the potential favourable effects suggested in refs. [7, 8]. Three, six, or twelve segments per row, displaced in a staggered arrangement, as sketched in Fig.1, have been considered ($l = 50\,, 25$, or $12.5\,mm$, respectively). Tests with truncated ribs were performed for the intermediate rib size only (e = 3 mm) and considering a fixed number of rows of rib segments (N = 20, corresponding to a rib pitch P = 25 mm). Figure 6 shows how *Nu* results are affected by the rib truncation at a given *Ra* number. Measured data refer to the inter-rib region only between rows since the free portions of the heated baseplate between the truncated pieces in each row are not optically accessible, as they are shadowed by rib segments.

Truncating the ribs generally increases the heat transfer performance throughout the majority (or the totality) of the inter-rib regions, as compared with the smooth plate geometry. An optimized number of segments per row is likely to exist; within the explored range of parameters for truncated ribs, the heat transfer rate from the surface is maximized with six rib segments per row ($l = 25$ mm), which corresponds to a segment length to rib pitch ratio (*l/P*) equal to 1.

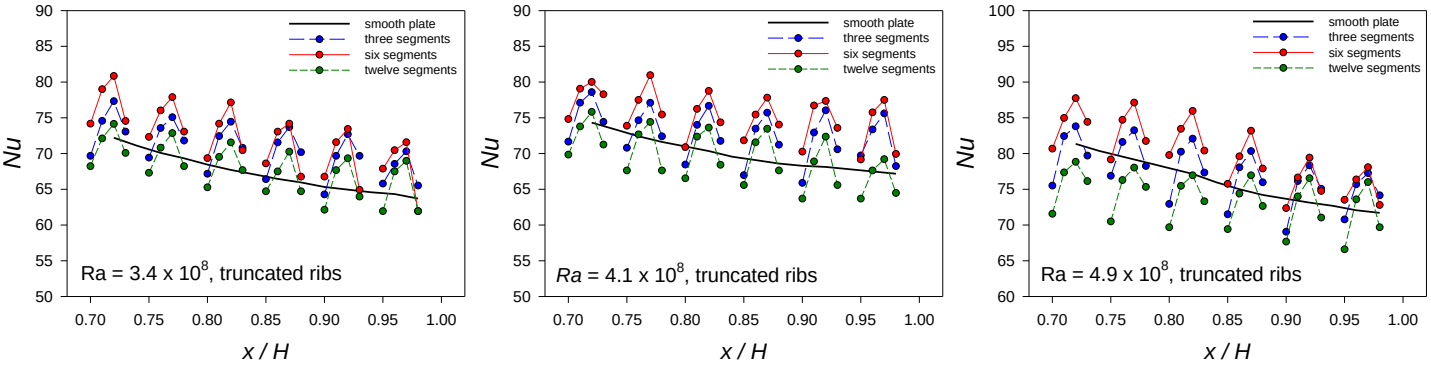

Figure 6. Nusselt number for ribbed (truncated ribs) and smooth plate: effect of the rib truncation.

3.1.4. Module-averaged Nusselt number

In order to quantify the relative merit (or demerit) of each rib configuration, local *Nu* values recorded within each inter-rib region have been averaged in order to obtain a module-averaged *Nu*. Even though the result may be biased by the limited number of measuring points (from 3 to 5 for each inter-rib region), the module-averaged data, plotted in Fig.7 (where symbols corresponding to every module-averaged *Nu* have been conventionally located at the centre of the respective inter-rib region), reflect at a glance the increase or decrease in the heat transfer performance relative to the smooth plate case (solid line). Regardless of the *Ra* number, repeated continuous ribs having the largest size (e = 5 mm) and intermediate size (e = 3 mm) but with small pitch (N = 40) display the worst performances as compared with the smooth plate. Other continuous rib geometries perform better but always at a lower level than that observed for the smooth plate. A general trend towards a progressive attenuation of the decrease in the heat transfer performance is observed as the trailing edge of the plate is approached. As attention is turned to truncated ribs, an increased module-averaged value of

Nu (as compared to the smooth plate case) occurs for two (out of three) truncated rib configurations, (namely those having three or six segments per row), even from a locally-averaged standpoint.

Table 2 shows the deterioration or the enhancement (relative to the smooth plate) provided by continuous and truncated ribs for all the explored configurations; the table is indicative of values averaged (for both the smooth and ribbed plate) over the top 30% of the heated plate, as only this region was included in the field of view of the schlieren device. As it emerges from inspection of the table, continuous ribs have a negative impact on the heat transfer performance, with degradations of the average Nusselt number up to 30%, relative to the smooth plate case. Conversely, the truncated ribs, arranged in a staggered pattern, yield a mild improvement (up to +8%), especially when a proper number of segments per row is chosen: in fact, while no significant variations, with respect to the smooth plate, are recorded for the truncated ribs with twelve segments per row, truncating the rib into three segments per row leads to a 2−5% *Nu* enhancement, which increases to 5−8% when six segments per row are considered.

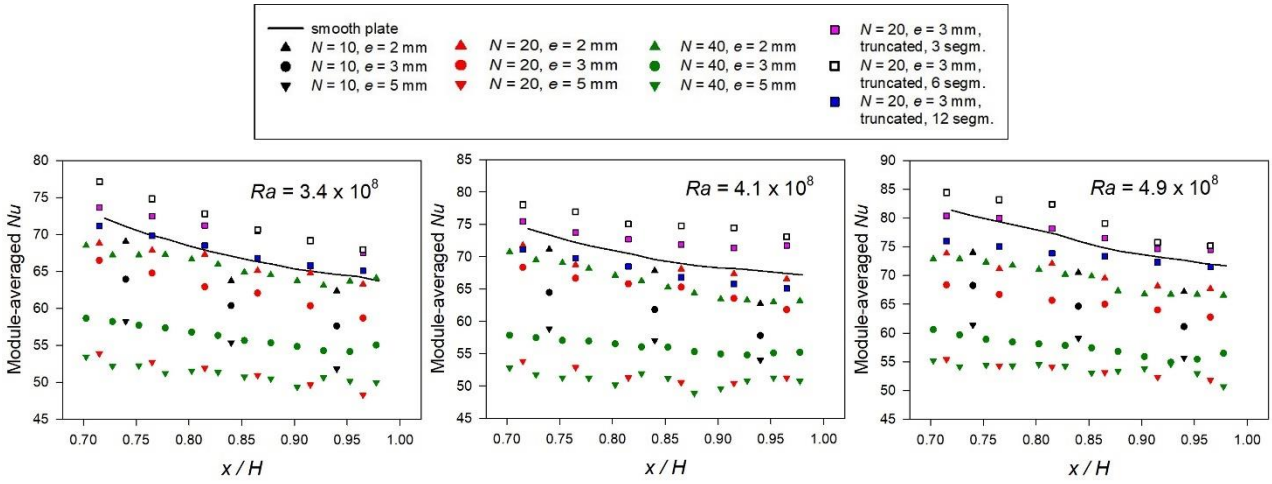

Figure 7. Module-averaged Nusselt number for ribbed and smooth plate.

Table 2. Ratio between average Nusselt numbers for the ribbed (only inter-rib regions) and the smooth plate. Only the top 30% of the heated plate is considered.

Rib type	Number of rib rows N	e (mm)	Number of truncated ribs per row	*Nusselt number ratio (ribbed vs. smooth plate)*		
				Ra=3.4 × 10^8	Ra=4.1 × 10^8	Ra=4.9 × 10^8
continuous	10	2	-	0.97	0.96	0.93
continuous	20	2	-	0.98	0.98	0.85
continuous	40	2	-	0.98	0.95	0.77
continuous	10	3	-	0.90	0.88	0.85
continuous	20	3	-	0.93	0.93	0.86
continuous	40	3	-	0.84	0.80	0.76
continuous	10	5	-	0.82	0.81	0.77
continuous	20	5	-	0.76	0.74	0.70
continuous	40	5	-	0.76	0.73	0.71
truncated	20	3	3	**1.05**	**1.04**	**1.02**
truncated	20	3	6	**1.07**	**1.08**	**1.05**
truncated	20	3	12	**1.01**	0.99	0.97

3.2 Boundary layer visualizations and air temperature fluctuations

The schlieren technique, based on a focal filament filter, allows a visualization of the boundary layer along the heated plate. In fact, when the filament is placed at the focus of the schlieren mirror, the points of the test section characterised by a non-zero thermal gradient (in the horizontal direction) appear bright in the schlieren image, while the undisturbed fluid region is coloured by the same colour of the filament (violet, as corresponding light rays are intercepted by the focal filament).

Figure 8 shows schlieren images of the boundary layers growing along the heated plate, without ribs and with continuous ribs having the same rib pitch (50 mm) and increasing rib size (2, 3, and 5 mm). All images refer to the largest Rayleigh number ($Ra = 4.9 \times 10^8$); a two-dimensional 1 cm × 1 cm grid has been superimposed to provide a dimensional reference (about the top 10 cm of the plate are framed in the images).

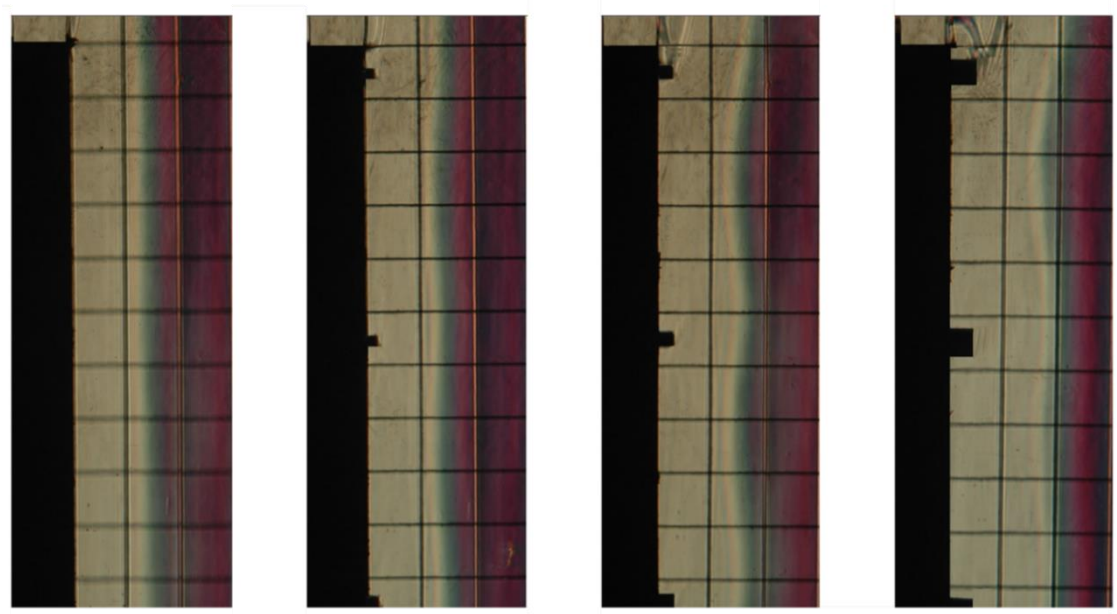

Figure 8. Schlieren images giving a qualitative representation of thermal boundary layer for the smooth plate and the ribbed plate (continuous ribs at different rib size).

Inspection of Fig.8 reveals that the boundary layer, almost flat along the top region of the smooth plate, becomes wavy when ribs are arranged over the plate, and the waviness amplitude is accentuated as the rib size increases. The effect of the ribs' density on the boundary layer is illustrated in Fig.9, where 3-mm-ribs with pitches of 50, 25, and 12.5 mm are considered: schlieren images show that the boundary layer progressively returns to exhibit a flat profile as the density of ribs placed on the baseplate increases.

It is worth noting that the images shown in Figs.8 and 9 were affected by low-frequency unsteady disturbances which are probably related to uncontrolled air currents in the laboratory room (the Rayleigh number was relatively large but not enough to depart from the laminar regime, for the case of the smooth plate); these instabilities were more pronounced when truncated ribs (with six segments) were considered. Figure 10 shows three different schlieren images of the filament shadow

(focal filament set at 0.35 mm from the focus) taken, on different time instants, for the truncated ribs (six segments per row): the line (filament shadow) projected on the camera, very close to the end of the boundary layer, has periodic disturbances at low frequency, with cycles of several seconds (left-hand and central picture), before recovering a quasi-steady behaviour (right-hand picture).

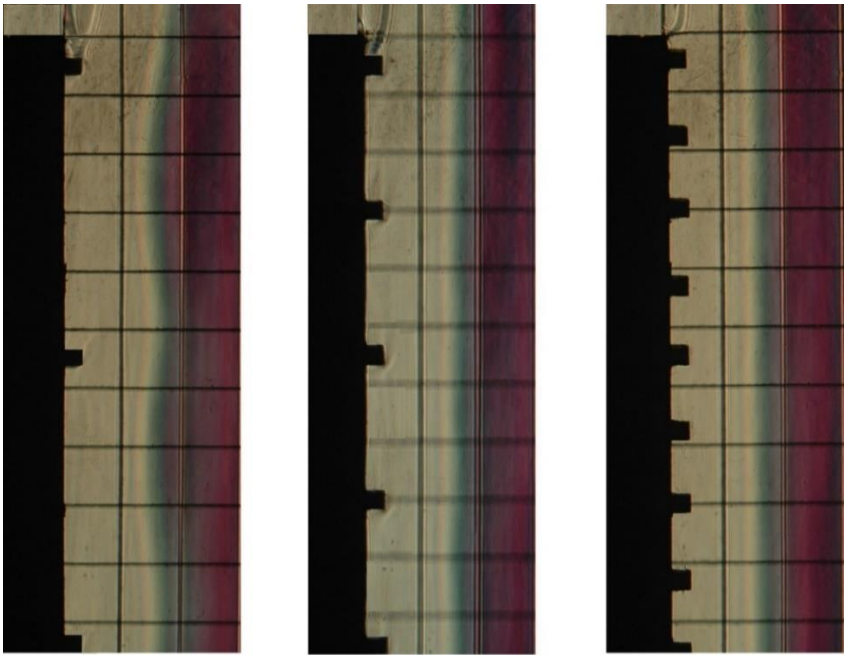

Figure 9. Schlieren images giving a qualitative representation of thermal boundary layer for the plate with continuous ribs at different rib pitch.

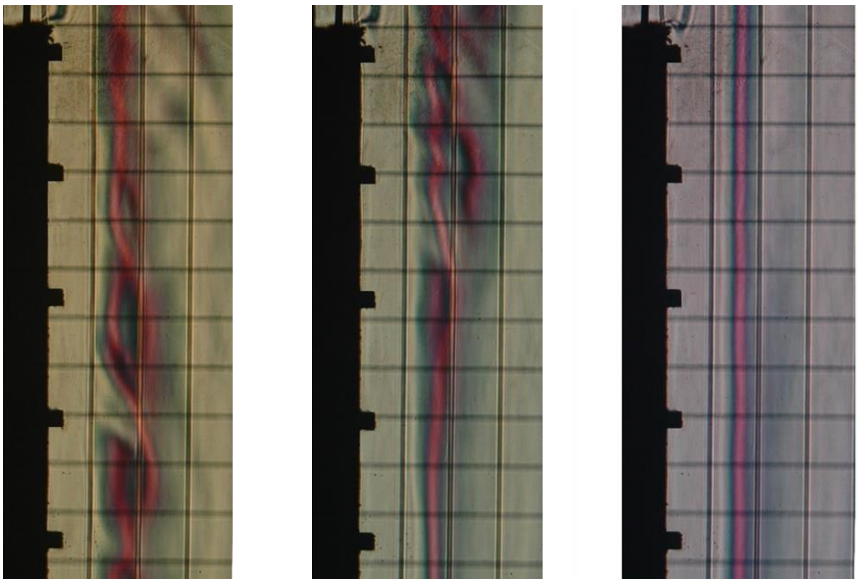

Figure 10. Examples of schlieren images showing the focal filament shadow (focal filament shifted by 0.35 mm from the focus) during low-frequency flow instabilities (truncated ribs, six segments per row).

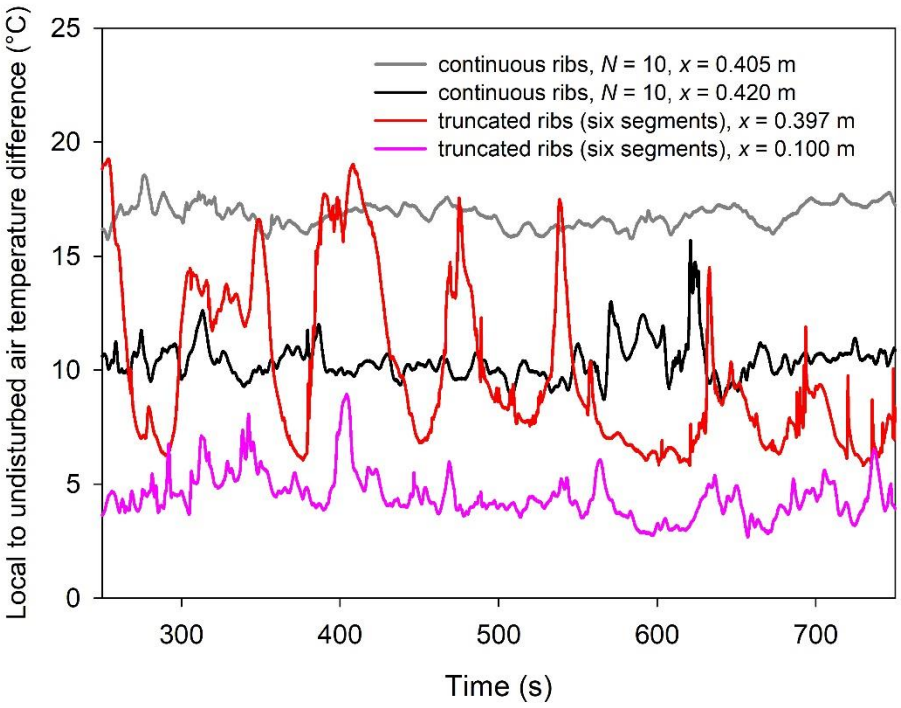

Figure 11. Traces of air temperature fluctuations, recorded at a 5 mm-distance from the heated plate and different elevations x, for the ribbed plate with continuous ribs (e = 3 mm, N = 10) and the ribbed plate with truncated ribs (e = 3 mm, N = 20 and six segments per row); $Ra = 4.9 \times 10^8$.

Local air temperature measurements, performed at different elevations and distances from the heated plate, confirmed the schlieren observations. Figures 11 and 12 display the time history of the local to undisturbed air temperature difference and the root-mean-square of its fluctuations (normalized by the wall-to-ambient temperature difference) at various distances from the heated plate, respectively. Air temperature fluctuations shown in Fig.11 were recorded at a 5 mm distance from the heated plate, approximately in the centre of the plate along the spanwise direction, and at different elevations, namely at 10 cm from the leading edge and at 8-10 cm to the trailing edge. For truncated ribs, the sensor was aligned to a row of rib segments and in the vicinity (within 1−2 mm) of the side face of a segment where the instabilities, if any, are likely to be induced. For continuous ribs, air temperature fluctuations were detected at elevations immediately downstream of the rib (x = 0.405) and in the inter-rib region (x = 0.420). Data refer to the highest Rayleigh number ($Ra = 4.9 \times 10^8$) and to ribs having a size of 3 mm. For the continuous ribs, the air temperature fluctuations were statistically confined within 2% of the wall-to-ambient temperature difference (with a larger attenuation in the stagnation zone, at x = 0.405 m), while temperature fluctuations registered for the truncated ribs with six segments, about at the same measurement elevation (x = 0.397 m) and same imposed wall-to-ambient temperature difference conditions, have a significantly larger magnitude. The amplification of disturbances was sensitive to the elevation (i.e., to the local Rayleigh number) as it was not observed close to the leading edge (x = 0.1 m). This circumstance is more evident from inspection of Fig.12, where the distributions of the root-mean-square of the air temperature fluctuations (normalized by the wall-to-ambient temperature difference) along the coordinate normal

to the heated plate, are reported for the smooth plate, continuous ribs, and truncated ribs with 3, 6, and 12 segments per row. Results show a peaked profile for truncated ribs with six segments, at the measurement station close to the trailing edge (x = 0.397 m) and in the vicinity of the segment side face, over the whole explored range of Ra based on plate height H (only points at the lowest and highest Ra are plotted), while fluctuations are markedly lower when detected again in the vicinity of the segment side face but close to the leading edge of the plate (x = 0.100 m). Measurements taken for truncated ribs with three and twelve segments per row, at the same vertical and spanwise coordinates, as well as those obtained for continuous ribs and the smooth plate, are characterised by markedly lower mean air temperature fluctuations at any distance from the heated plate. Even though air temperature fluctuation intensity (9% at the most), registered for truncated ribs with six segments, remains below values that are typically experienced when the transitional and turbulent regimes take place [31], it can be argued that the boundary layer growing along the truncated ribs (with six segments) interacts with, filters and amplifies the exogenous environmental disturbances sufficiently far away from the leading edge of the plate, thus yielding a possible explanation for the larger heat transfer coefficients measured, compared with those recorded for all other explored geometries.

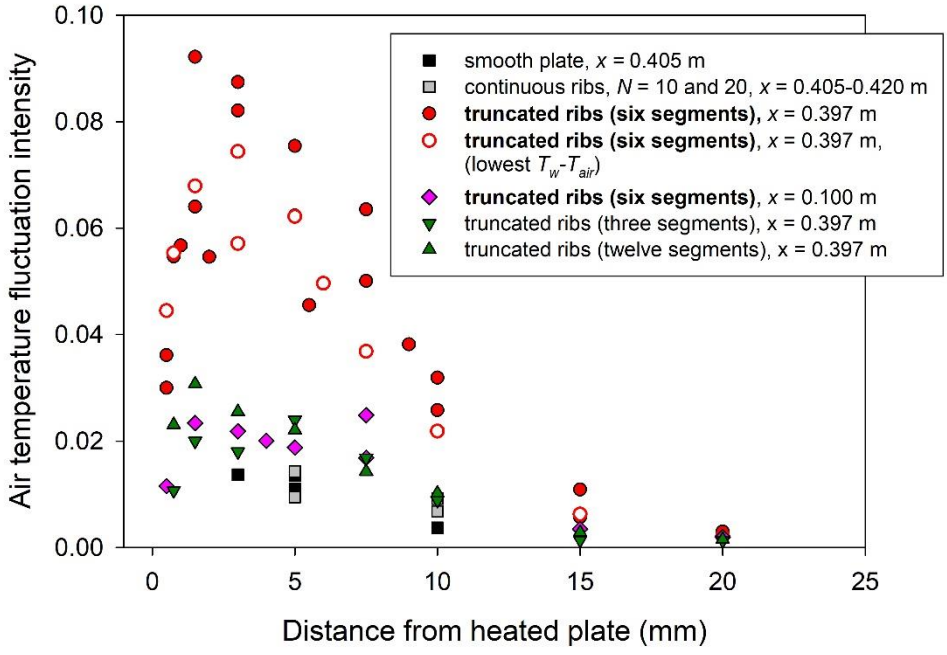

Figure 12. Intensity of air temperature fluctuations, at different distances from the heated plate and at different elevations x, for the smooth plate, the ribbed plate with continuous ribs (e = 3 mm, N = 10 and 20), and the ribbed plate with truncated ribs (e = 3 mm, N = 20 and 3, 6, and 12 segments per row). All data refer to the highest wall-to-ambient air temperature difference $T_w - T_{air}$ (Ra = 4.9 × 10^8) except for data indicated with empty circles, recorded for the lowest $T_w - T_{air}$ (Ra = 3.4 × 10^8).

4. Conclusions

The natural convection heat transfer from a ribbed vertical plate was experimentally investigated by varying the rib size and pitch and by considering the effect of rib truncation. The schlieren optical technique was employed as a diagnostic tool to estimate the heat transfer coefficient along the vertical plate. The main conclusions of this research are summarized below:

i. Compared to a smooth, isothermal, vertical surface, the presence of continuous ribs negatively affects the heat transfer performance within the range of variation of the parameters investigated, with degradations of the average Nusselt number up to 30%, relative to the smooth plate case. Only a local heat transfer enhancement in the inter-rib region was found for a relatively high rib pitch-to-height ratio (higher than 10), counterbalanced by a marked reduction immediately downstream and upstream of ribs due to the presence of stagnation regions.

ii. When continuous ribs are replaced by truncated ribs displaced in a staggered arrangement, significant heat transfer enhancements, relative to the smooth surface, were noticed throughout the majority, or the totality, of the inter-rib regions. To the authors' knowledge, this is the first time that this effect is documented. From the average point of view, the truncated ribs yield a mild improvement (up to +8%), with the best heat transfer performance obtained for a value of the number of segments per row (six) intermediate in the explored range (three to twelve), suggesting the presence of an optimal length of the rib segments, for given rib size and pitch, that maximizes the heat transfer enhancement.

iii. Supplementary air temperature measurements performed at short distances from the heated test plate showed that truncated ribs of a given value of the segment length (corresponding to the maximum heat transfer performance) induce fluctuations much larger than those occurring for the rest of the experimental campaign. The reason why the truncated rib arrangement yields enhanced heat transfer on the vertical smooth surface is likely related to either the more efficient redistribution of buoyant airflow within the laminar flow regime or to a premature transition to turbulence induced by rib truncation, as large-amplitude air temperature fluctuations suggest.

References

[1] T. Fujii, M. Fujii, M. Takeuchi, Influence of various surface roughness on the natural convection, International Journal of Heat and Mass Transfer 16 (1973) 629−640. https://doi.org/10.1016/0017-9310(73)90228-7

[2] S. H. Bhavnani, A. E. Bergles, Effect of surface geometry and orientation on laminar natural convection heat transfer from a vertical flat plate with transverse roughness elements, International Journal of Heat and Mass Transfer 33 (1990) 965−981. https://doi.org/10.1016/0017-9310(90)90078-9

[3] G. Tanda, Natural convection heat transfer in vertical channels with and without transverse square ribs, International Journal of Heat and Mass Transfer 40 (1997) 2173−2185. https://doi.org/10.1016/S0017-9310(96)00246-3

[4] G. Tanda, Natural convective heat transfer in vertical channels with low-thermal-conductivity ribs, International Journal of Heat and Fluid Flow 29 (2008) 1319−1325. https://doi.org/10.1016/j.ijheatfluidflow.2008.05.004

[5] J. Hærvig, H. Sørensen, Natural convective flow and heat transfer on unconfined isothermal zigzag-shaped ribbed vertical surfaces, International Communications in Heat and Mass Transfer 119 (2020) 104982. https://doi.org/10.1016/j.icheatmasstransfer.2020.104982

[6] B. Nghana, F. Tariku, G. Bitsuamlak, Numerical assessment of the impact of transverse roughness ribs on the turbulent natural convection in a BIPV air channel, Building and Environment 217 (2022) 109093. https://doi.org/10.1016/j.buildenv.2022.109093

[7] S. H. Bhavnani, A. E. Bergles, Natural convection heat transfer from sinusoidal wavy surfaces, Wärme- und Stoffübertragung 26 (1991) 341−349. https://doi.org/10.1007/BF01591667

[8] L.-S. Yao, Natural convection along a vertical complex wavy surface, International Journal of Heat and Mass Transfer 49 (2006) 281–286. https://doi.org/10.1016/j.ijheatmasstransfer.2005.06.026

[9] D. Cavallero, G. Tanda, An experimental investigation of forced convection heat transfer in channels with rib turbulators by means of liquid crystal thermography, Experimental Thermal and Fluid Science 26 (2002) 115–121. https://doi.org/10.1016/S0894-1777(02)00117-6

[10] S. U. Onbasioglu, H. Onbaşıoğlu, On enhancement of heat transfer with ribs, Applied Thermal Engineering 24 (2004) 43–57. https://doi.org/10.1016/S1359-4311(03)00216-3

[11] M. Imbriale, M. Panelli, G. Cardone, Heat transfer enhancement of natural convection with ribs, Quantitative InfraRed Thermography 9 (2012) 55–67. http://dx.doi.org/10.1080/17686733.2012.681881

[12] E. M. Smirnov, A. G. Abramov, A. A. Smirnovsky, P. E. Smirnov, Numerical simulation of turbulence arising in the free convection boundary layer after a cross row of rectangular obstacles,

Journal of Physics: Conf. Series 1128 (2018) 012090. http://dx.doi.org/10.1088/1742-6596/1128/1/012090

[13] G. Tanda, Experiments on natural convection in water-cooled ribbed channels with different aspect ratios, International Journal of Heat and Mass Transfer 110 (2017) 606−612. https://doi.org/10.1016/j.ijheatmasstransfer.2017.03.050

[14] W. Hauf, U. Grigull, Optical Methods in Heat Transfer, in: J. P. Hartnett, T. F. Irvine, Jr. (Eds.), Adavances in Heat Transfer, Academic Press, 1970, 6, pp. 133−366.

[15] W. Merzkirch, Flow Visualization, Academic Press, 1974.

[16] H. Kleine, H. Grönig, K. Takayama, Simultaneous shadow, schlieren and interferometric visualization of compressible flows, Optics and Lasers in Engineering 44 (2006) 170–189. https://doi.org/10.1016/j.optlaseng.2005.04.009

[17] D. Ambrosini, G. Tanda, Comparative measurements of natural convection heat transfer in channels by holographic interferometry and schlieren, European Journal of Physics 27 (2006) 159−172. https://doi.org/10.1088/0143-0807/27/1/016

[18] M. J. Hargather, G. S. Settles, A comparison of three quantitative schlieren techniques, Optics and Lasers in Engineering 50 (2012) 8–17. https://doi.org/10.1016/j.optlaseng.2011.05.012

[19] M. Raffel, Background-oriented schlieren (BOS) techniques, Experiments in Fluids 56 (2015) 60. https://doi.org/10.1007/s00348-015-1927-5

[20] D. S. Jain, S. S. Rao, A. Srivastava, Rainbow schlieren deflectometry technique for nanofluid-based heat transfer measurements under natural convection regime, International Journal of Heat and Mass Transfer 98 (2016) 697–711. http://dx.doi.org/10.1016/j.ijheatmasstransfer.2016.03.062

[21] G. S. Settles, Smartphone schlieren and shadowgraph imaging, Optics and Lasers in Engineering 104 (2018) 9–21. http://dx.doi.org/10.1016/j.optlaseng.2017.07.002

[22] A. Vyas, B. Mishra, A. Agrawal, A. Srivastava, Non-intrusive investigation of flow and heat transfer characteristics of a channel with a built-in circular cylinder, Physics of Fluids 30 (2018) 033602. https://doi.org/10.1063/1.5009427

[23] J. M. Schulz, H. Junne, L. Böhm, M. Kraume, Measuring local heat transfer by application of Rainbow Schlieren Deflectometry in case of different symmetric conditions, Experimental Thermal and Fluid Science 110 (2020) 109887. https://doi.org/10.1016/j.expthermflusci.2019.109887

[24] G. Tanda, Natural convection heat transfer from a staggered vertical plate array, ASME Journal of Heat Transfer 115 (1993) 938−945. https://doi.org/10.1115/1.2911390

[25] F. Devia, G. Milano, G. Tanda, Evaluation of thermal field in buoyancy-induced flows by a schlieren method, Experimental Thermal and Fluid Science 8 (1994) l−9. https://doi.org/10.1016/0894-1777(94)90067-1

[26] G. Tanda, F. Devia, Application of a schlieren technique to heat transfer measurements in free-convection, Experiments in Fluids 24 (1998) 285–290. https://doi.org/10.1007/s003480050175

[27] G. Tanda, M. Fossa, M. Misale, Heat transfer measurements in water using a schlieren technique, International Journal of Heat and Mass Transfer 71 (2014) 451–458. http://dx.doi.org/10.1016/j.ijheatmasstransfer.2013.12.022

[28] R. J. Goldstein, Optical Techniques for Temperature Measurement, in: E. R. G. Eckert, R. J. Goldstein (Eds.), Measurements in Heat Transfer, second ed., Hemisphere Publishing Corporation, 1976, 5.

[29] F. Devia, G. Tanda, Investigation of natural convection heat transfer from a horizontal isothermal plate by schlieren tomography, Heat and Technology 18 (2000) 41−46.

[30] G. D. Raithby, K. G. T. Hollands, Natural Convection, in: W. M. Rohsenow, J. P. Hartnett, E. N. Ganić (Eds.), Handbook of Heat Transfer Fundamentals, second ed., McGraw Hill, 1985, 6.

[31] T. Tsuji, Y. Nagano, Characteristics of a turbulent natural convection boundary layer along a vertical flat plate, International Journal of Heat and Mass Transfer 31 (1988) 1723−1734. https://doi.org/10.1016/0017-9310(88)90284-0

[32] S. Ostrach, An analysis of laminar free-convection flow and heat transfer about a flat plate parallel to the direction of the generating body force, NACA Report No 1111, 1953.

[33] F. Godaux, B. Gebhart, An experimental study of the transition of natural convection flow adjacent to a vertical surface, International Journal of Heat and Mass Transfer 17 (1974) 93−107. https://doi.org/10.1016/0017-9310(74)90042-8

[34] A. Bejan, J. L. Lage, The Prandtl number effect on the transition in natural convection along a vertical plate, ASME Journal of Heat Transfer 112 (1990) 787−790. https://doi.org/10.1115/1.2910457

[35] R. Cheesewright, Turbulent natural convection from a vertical plane surface, ASME Journal of Heat Transfer 90 (1968) 1−6. https://doi.org/10.1115/1.3597453

[36] M. Schaub, M. Kriegel, S. Brandt, Experimental investigation of heat transfer by unsteady natural convection at a vertical flat plate, International Journal of Heat and Mass Transfer 136 (2019) 1186–1198. https://doi.org/10.1016/j.ijheatmasstransfer.2019.03.089

[37] S. W. Churchill, H. S. Chu, Correlating equations for laminar and turbulent free convection from a vertical plate, International Journal of Heat and Mass Transfer 18 (1975) 1323–1329. https://doi.org/10.1016/0017-9310(75)90243-4

[38] E. N. Ahmed, A. Bottaro, G. Tanda, A homogenization approach for buoyancy-induced flows over micro-textured vertical surfaces, Journal of Fluid Mechanics 941 (2022) A53. https://doi.org/10.1017/jfm.2022.320